Nano Research 2017, 10(4): 1107–1114
DOI 10.1007/s12274-016-1415-0
Research Article
ISSN 1998-0124
CN 11-5974/O4

Structural, optical, and electrical properties of phase-controlled cesium lead iodide nanowires

Minliang Lai[1], Qiao Kong[1], Connor G. Bischak[1], Yi Yu[1,2], Letian Dou[1,2], Samuel W. Eaton[1], Naomi S. Ginsberg[1,2,3,4,5], and Peidong Yang[1,2,3,6] (✉)

[1] *Department of Chemistry, University of California, Berkeley, California 94720, USA*
[2] *Materials Sciences Division, Lawrence Berkeley National Laboratory, Berkeley, California 94720, USA*
[3] *Kavli Energy Nanosciences Institute, Berkeley, California 94720, USA*
[4] *Molecular Biophysics and Integrative Bioimaging Division, Lawrence Berkeley National Laboratory, Berkeley, California 94720, USA*
[5] *Department of Physics, University of California, Berkeley, California 94720, USA*
[6] *Department of Materials Science and Engineering, University of California, Berkeley, California 94720, USA*

Received: 7 November 2016
Revised: 10 December 2016
Accepted: 12 December 2016

KEYWORDS
inorganic halide perovskite,
$CsPbI_3$,
phase transition,
stability

ABSTRACT

Cesium lead iodide ($CsPbI_3$), in its black perovskite phase, has a suitable bandgap and high quantum efficiency for photovoltaic applications. However, $CsPbI_3$ tends to crystalize into a yellow non-perovskite phase, which has poor optoelectronic properties, at room temperature. Therefore, controlling the phase transition in $CsPbI_3$ is critical for practical application of this material. Here we report a systematic study of the phase transition of one-dimensional $CsPbI_3$ nanowires and their corresponding structural, optical, and electrical properties. We show the formation of perovskite black phase $CsPbI_3$ nanowires from the non-perovskite yellow phase through rapid thermal quenching. Post-transformed black phase $CsPbI_3$ nanowires exhibit increased photoluminescence emission intensity with a shrinking of the bandgap from 2.78 to 1.76 eV. The perovskite nanowires were photoconductive and showed a fast photoresponse and excellent stability at room temperature. These promising optical and electrical properties make the perovskite $CsPbI_3$ nanowires attractive for a variety of nanoscale optoelectronic devices.

1 Introduction

Organic–inorganic hybrid perovskites, such as $CH_3NH_3PbI_3$, have recently stimulated great interest in the photovoltaic and optoelectronic fields as they demonstrate improved power conversion efficiencies and can be fabricated using low-cost solution processes [1–4]. Although the efficiency of hybrid perovskite photovoltaic devices has exceeded 20%, the organic cation MA^+ is susceptible to environmental degradation from moisture and heat [5–8].

Recently, all-inorganic nanoscale perovskite structures

Address correspondence to p_yang@berkeley.edu

($CsPbX_3$), including quantum dots, nanowires, and nanoplates, have been obtained using colloidal synthesis or low temperature solution processing [9–12]. These nanostructured inorganic perovskites show greatly improved stability, as well as promising optical and electrical properties [11, 13]. Among these materials, $CsPbI_3$ shows the unique combination of a suitable bandgap, high quantum efficiency, and long radiative lifetime for photovoltaic applications [11]. The black perovskite phase (B-$CsPbI_3$) is stable above 300 °C [14, 15] and shows the desired photovoltaic behavior. This material undergoes a phase transition to a yellow non-perovskite phase (Y-$CsPbI_3$) with poor optoelectronic properties upon cooling to room temperature [16]. The transformation into the yellow phase limits further fundamental studies and applications of the desired black phase. Therefore, enhancing the stability of the black $CsPbI_3$ phase at room temperature has attracted great interest. A colloidal synthesis method yielded meta-stable black $CsPbI_3$ nanocrystals, but these recrystallized to the yellow phase upon extended storage or removal of capping ligands [9, 17]. Recently, a new purification process was reported to reduce the loss of ligands on the $CsPbI_3$ quantum dot surface and to increase the stability of the black phase under ambient storage [18]. Chloride doping has also been shown to enhance the stability of perovskite phase $CsPbI_3$, but the effect of chloride incorporation requires further investigation [19]. In order to stabilize the black $CsPbI_3$ phase more effectively, the intrinsic phase transition behavior of this material should be systematically investigated, which has not yet been undertaken.

One-dimensional (1D) nanowires (NWs) are considered a good platform for studying solid–solid phase transitions [20]. NWs are single crystals with the advantage of a controllable morphology, which can eliminate the contribution of domain boundaries and morphological variation [21]. In addition, as the size of the material is reduced to the nanoscale, NWs can show enhanced phase stability, and possess optoelectronic properties superior to those of bulk counterparts [22, 23]. Therefore, understanding the phase transition of $CsPbI_3$ nanowires not only reveals intrinsic properties of the material, but also enables the development of nanostructures for photonic and electrical devices.

Here we report a systematic study of the structural phase transition of $CsPbI_3$ nanowires between the yellow and black phases. The corresponding dramatic structural change induced significant differences in the optical and electronic properties. The B-$CsPbI_3$ nanowires showed about a 100-fold increase in photoluminescent emission efficiency and a decrease in the bandgap from 2.78 to 1.76 eV, compared to Y-$CsPbI_3$. Unlike Y-$CsPbI_3$, B-$CsPbI_3$ nanowires showed strong photoconductance and a fast photoresponse, demonstrating potential for photovoltaic and photodetector applications. B-$CsPbI_3$ nanowires exhibited excellent stability when stored in an inert atmosphere.

2 Experimental

$CsPbI_3$ nanowires were synthesized using a surfactant-free solution process, by dipping a PbI_2 film into a CsI-methanol solution (for additional details, see the Electronic Supplementary Material (ESM)). From scanning electron microscopy (SEM) analysis (Fig. 1(a)), it can be seen that the product contained only nanowires, which formed a mesh network. The diameter of the $CsPbI_3$ nanowires could be adjusted by changing the concentration of the CsI-methanol solution (Fig. S1 in the ESM). The X-ray diffraction (XRD) patterns of the as-grown nanowires were assigned to the non-perovskite orthorhombic phase Y-$CsPbI_3$ (Fig. 1(b)); no patterns from the PbI_2 or CsI starting materials were observed. The PbI_6 octahedra are edge-shared in Y-$CsPbI_3$, forming a 1D chain structure along the [010] direction (Fig. 1(c)). The anisotropic crystal structure was attributed to the growth of the nanowires in a preferred direction. Selected area electron diffraction (SAED) of individual nanowires further indicated that the as-grown nanowires were single crystalline and the growth direction of the non-perovskite phase was [010] (Fig. 1(d) and Fig. S2 in the ESM).

In order to achieve the phase transition to the perovskite phase, the Y-$CsPbI_3$ nanowire film was heated up to 310 °C for 10 min in a glovebox; the color change from yellow to black was observed (Figs. S3(a) and S3(b) in the ESM). The film remained black when the sample was rapidly quenched to room temperature (for details, see the ESM). The quenching rate was about

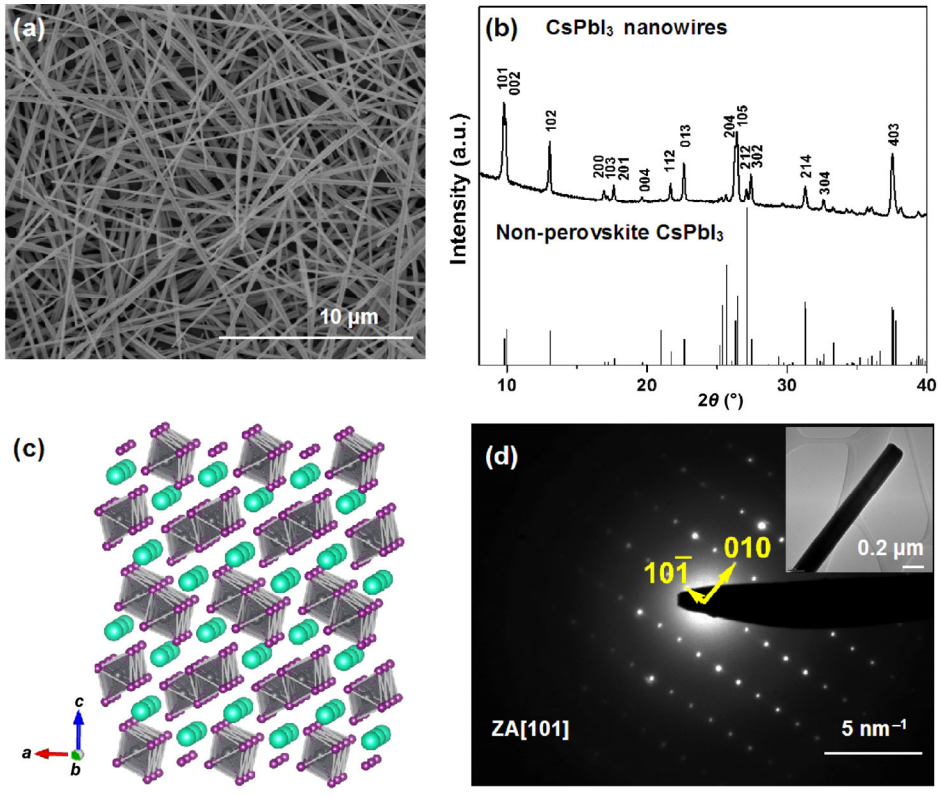

Figure 1 Synthesis and structural characterization of Y-$CsPbI_3$ nanowire mesh. (a) SEM image of the Y-$CsPbI_3$ nanowire mesh grown on a glass substrate. (b) XRD patterns of as-grown $CsPbI_3$ nanowire mesh with the standard diffraction pattern of the orthorhombic $CsPbI_3$ indicated by the dark lines. (c) Schematic diagram of the structure of Y-$CsPbI_3$ (grey = Pb atoms; purple = I atoms; green = Cs atoms). (d) SAED pattern of an individual nanowire confirming the orthorhombic $CsPbI_3$ phase. The inset shows a TEM image of the same nanowire.

150 ℃·s^{-1} (measured using an infrared thermometer). The XRD patterns of the black film showed no peaks corresponding to the Y-$CsPbI_3$ phase or any products from decomposed CsI and PbI_2, confirming the success of the phase transition (Fig. S5(a) in the ESM). However, the XRD patterns could not be assigned to the highly symmetric cubic phase, which has been observed *in situ* at 310 ℃ [24]. The obvious split peaks at about 14°, 20°, and 28° and the smaller peaks between 20° and 28° indicated a lower symmetry orthorhombic perovskite phase. Such a phase has been previously observed in nanostructured $CsPbI_3$ produced using an anion exchange reaction or chemical vapor deposition [25–27]. The structure of the orthorhombic perovskite phase is similar to the ideal cubic phase, where PbI_6 octahedra are slightly distorted and corner-shared in three dimensions (Fig. 2(a)). $CsPbI_3$ should be in an ideal cubic phase at 310 ℃, but the lattice probably relaxed and distorted during the quenching process, forming an orthorhombic perovskite structure. The crystal structure of individual B-$CsPbI_3$ nanowires was further confirmed by transmission electron microscopy (TEM) characterization (Fig. 2(b)). Additional TEM analysis is provided in Fig. S4 (in the ESM). In addition, simulated XRD patterns based on the B-$CsPbI_3$ structure matched our experimental patterns (Fig. S5(b) in the ESM). Therefore, both XRD and TEM characterizations confirmed that the $CsPbI_3$ nanowires underwent a structural phase transition from the non-perovskite phase to a perovskite phase, where the perovskite phase could be stabilized by fast thermal quenching.

3 Results and discussion

The different crystal structures of the Y-$CsPbI_3$ and B-$CsPbI_3$ phases result in distinct band structures and optical properties. The PL spectrum of the Y-$CsPbI_3$ nanowires showed two broad peaks centered at

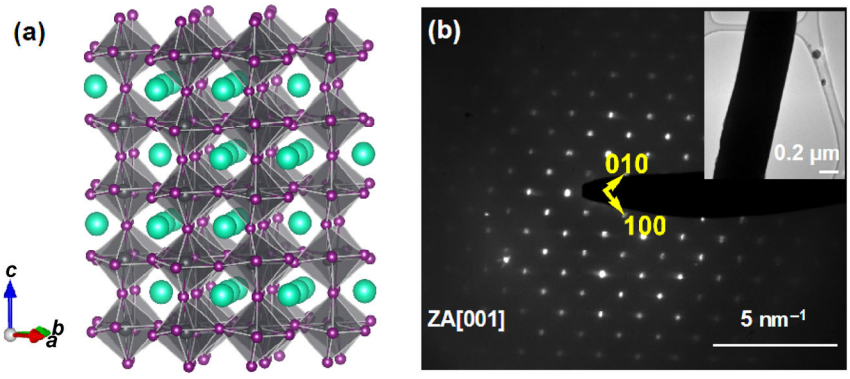

Figure 2 Structural characterization of B-$CsPbI_3$. (a) Schematic diagram of the structure of the black orthorhombic $CsPbI_3$; the PbI_6 octahedra are slightly distorted compared to the ideal cubic perovskite structure. (b) SAED patterns of an individual B-$CsPbI_3$ nanowire, which match the simulated black orthorhombic phase well. The scale bar is 5 nm^{-1}. The inset shows a TEM image of the same nanowire.

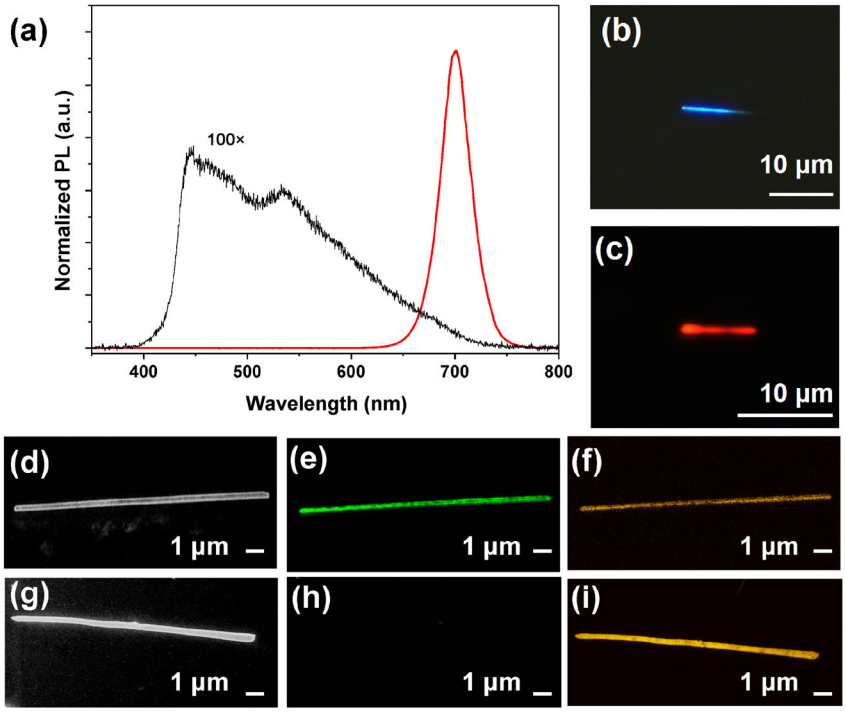

Figure 3 Comparison of the optical properties of Y-$CsPbI_3$ and B-$CsPbI_3$ nanowires. (a) Normalized PL of a Y-$CsPbI_3$ (black line) and a B-$CsPbI_3$ (red line) nanowire under the same laser excitation power; the Y-$CsPbI_3$ intensity was 100 times higher than that of the B-$CsPbI_3$. (b) and (c) Optical PL images of a Y-$CsPbI_3$ and B-$CsPbI_3$ nanowire, respectively. (d) and (g) SEM images of a Y-$CsPbI_3$ and B-$CsPbI_3$ nanowire, respectively. The corresponding cathodoluminescence images ((e) and (h)) showing emission using an 85 nm band-pass filter centered at 510 nm (in false green color) and ((f) and (i)) with a 50 nm band-pass filter centered at 700 nm (in false yellow color).

about 450 and 530 nm (Fig. 3(a)), which was similar to that observed for $CsPbI_3$ nanowires that we synthesized previously using a colloidal method [10]. The high-energy peak likely comes from excitonic emission, while the low-energy peak is probably due to self-trapped excitons (STEs) [10]. The formation of STEs probably results from strong exciton–phonon interaction in the 1D chain structure of the PbI_6 octahedral [28]. When the PbI_6 octahedral changed from a 1D double chain structure to a 3D network, the bandgap of the B-$CsPbI_3$ nanowires reduced from 2.79 to 1.76 eV. The PL intensity increased accordingly about 100-fold. Unlike the strong self-trapped emission in Y-$CsPbI_3$, B-$CsPbI_3$ nanowires showed dominant

band edge emission, indicating fewer excitonic traps in the perovskite structure [29]. In order to better characterize the spatial distribution of emissive sites of individual Y-$CsPbI_3$ and B-$CsPbI_3$ nanowires, we used cathodoluminescence microscopy (CL). This technique provides excellent spatial resolution of the photon emitted from a sample when excited by a focused electron beam [30]. Since Y-$CsPbI_3$ nanowires exhibit a broad emission in the range 450–750 nm (Fig. S6(a) in the ESM), the CL mappings in the 467.5–552.5 and 675–725 nm ranges both showed uniform emission (Figs. 3(d)–3(f)). However, the B-$CsPbI_3$ nanowires showed only a narrow emission centered around 700 nm (Fig. S6(b) in the ESM). Therefore, the CL mapping of a single B-$CsPbI_3$ nanowire showed only uniform emission in the 675–725 nm range (Figs. 3(g)–3(i)). The absence of an emission signal from 467.5 to 552.5 nm indicates that the entire nanowire was converted to the B-$CsPbI_3$ phase.

The structural phase transition also significantly alters the electrical properties of the materials [31]. Considering this, we investigated the electrical properties of Y-$CsPbI_3$ and B-$CsPbI_3$ nanowires in darkness and under one sun (AM1.5) illumination. Individual Y-$CsPbI_3$ and B-$CsPbI_3$ nanowires were transferred to fabricated Au bottom contacts using a micromanipulator (Fig. 4(a)). All electrical measurements were carried out in a vacuum chamber at 77 K. Figure 4(b) shows the results of the conductance of individual Y-$CsPbI_3$ and B-$CsPbI_3$ nanowires in dark and illuminated conditions. The Y-$CsPbI_3$ nanowire was found to be insulating under dark conditions with a current of the order of 10^{-13} A at 10 V bias. Almost no photocurrent was detected when the Y-$CsPbI_3$ nanowire was illuminated. The poor photoconductance is consistent with previous reports of the non-functionality of Y-$CsPbI_3$ for photovoltaic applications [32]. The B-$CsPbI_3$ nanowire also showed high resistivity under dark conditions, but was several times more conductive than the Y-$CsPbI_3$ nanowire. The current under illumination increased about 100 times compared to the dark current, indicating a significant contribution

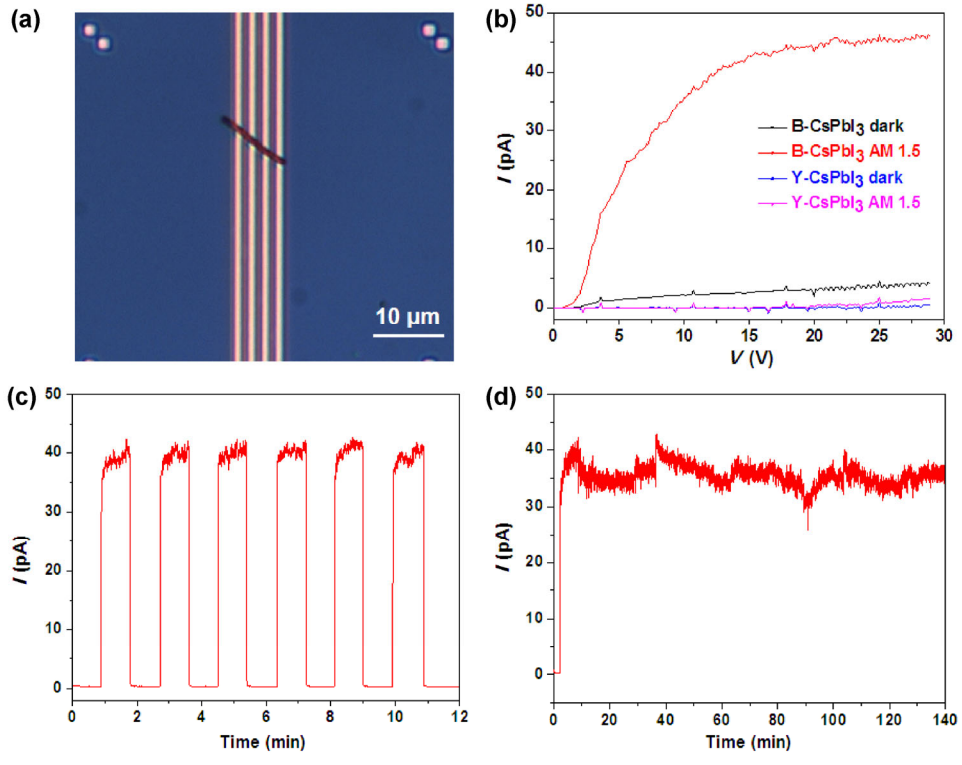

Figure 4 Electrical characterization of Y-$CsPbI_3$ and B-$CsPbI_3$ nanowires: (a) a nanowire transferred onto Au electrodes. The gap between the electrodes was 1 μm. (b) Conductance of the nanowires in darkness and under one sun (AM1.5) illumination (blue: dark Y-$CsPbI_3$; magenta: AM1.5 Y-$CsPbI_3$; black: dark B-$CsPbI_3$; red: AM1.5 B-$CsPbI_3$). (c) Photoresponse of B-$CsPbI_3$ measured under AM1.5 at 10 V and 77 K. (d) Stability of photocurrent under AM1.5 at 10 V and 77 K.

from the photogenerated carriers. The photoresponse of B-$CsPbI_3$ nanowires was fast, with an on/off conductance ratio of 10^2 (Fig. 4(c)). The photocurrent showed no significant decay, even when the device had been continuously illuminated for more than 2 h (Fig. 4(d)). Such excellent stability, along with the promising optoelectronic properties, makes the B-$CsPbI_3$ nanowires a promising material for device applications such as photovoltaics and photodetectors.

Figure 5 shows the stability of the B-$CsPbI_3$ nanowires in an inert atmosphere. The B-$CsPbI_3$ nanowires remained in the perovskite phase showing red PL emission for 4 weeks, indicating that their intrinsic stability is high. The excellent phase stability of the B-$CsPbI_3$ nanowires at room temperature was probably due to a strain effect from the rapid thermal quenching [33, 34]. Surface strain should be significant due to the large surface area of the NWs. The high-quality single crystal structure with a low defect density likely contributed to the phase stability. However, the mechanism for the excellent phase stability needs further investigation. Conventional phase-change memory materials, such as $Ge_2Sb_2Te_5$, produce metastable amorphous structures upon rapid thermal cooling, and transform to the stable crystalline structure after subsequent reheating [35]. Similarly, we found B-$CsPbI_3$ transitioned back to the yellow phase when reheated to 200 °C in a glovebox. This phase transition was also confirmed by XRD measurements (Fig. S8(a) in the ESM). The PL emission of a B-$CsPbI_3$ nanowire changed from red to weak blue after heating to about 200 °C, indicating a phase transition from B-$CsPbI_3$ to Y-$CsPbI_3$ (Figs. S8(b)–S8(d) in the ESM). Therefore, the B-$CsPbI_3$ nanowires were in a meta-stable phase at room temperature. Although the Y-$CsPbI_3$ phase is energetically favorable at room temperature, the B-$CsPbI_3$ phase can be kinetically trapped through the quenching process. At a temperature as high as 200 °C, B-$CsPbI_3$ nanowires gain enough thermal energy to overcome the thermodynamic barrier (around 4.4 $kJ \cdot mol^{-1}$) to convert to the yellow phase (Fig. S8(e) in the ESM). The bi-stability and reversibility of the black and yellow phases makes $CsPbI_3$ nanowires potentially useful in phase-transition memory devices [36, 37].

4 Conclusion

In summary, we systematically studied the structural phase transition and associated optical and electrical properties of non-perovskite Y-$CsPbI_3$ and perovskite B-$CsPbI_3$ nanowires. Perovskite B-$CsPbI_3$ nanowires showed a lower bandgap, stronger PL emission, and higher photoconductance than the Y-$CsPbI_3$ phase.

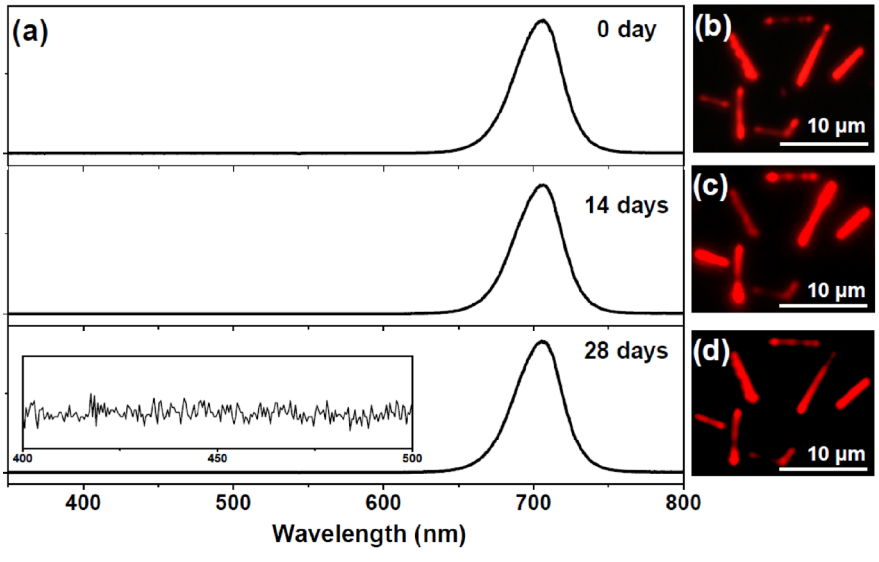

Figure 5 Excellent stability of B-$CsPbI_3$ nanowires in an inert atmosphere. (a) Normalized PL spectrum of as-fabricated B-$CsPbI_3$ nanowires, and after storage in a N_2-filled glovebox for 14 and 28 days. The inset shows the portion of the spectrum from 400 to 500 nm, indicating no PL emission from the Y-$CsPbI_3$. PL images of B-$CsPbI_3$ nanowires (b) as fabricated, (c) after 14 days, and (d) after 28 days.

Additionally, B-$CsPbI_3$ nanowires showed good stability at room temperature. This study unveiled important fundamental properties of the structural phase transition in $CsPbI_3$ nanowires. The ability to control the phase transition of this material thermally may be an advantage for future applications such as photovoltaic, photodetector, and memory devices.

Acknowledgements

This work was supported by the U.S. Department of Energy, Office of Science, Office of Basic Energy Sciences, Materials Sciences and Engineering Division, under Contract No. DE-AC02-05-CH11231 within the Physical Chemistry of Inorganic Nanostructures Program (KC3103). Work at the NCEM, Molecular Foundry was supported by the Office of Science, Office of Basic Energy Science, of the U.S. Department of Energy under Contract No. DE-AC02-05CH11231. Minliang Lai and Qiao Kong thank Suzhou Industrial Park for the fellowship support. Connor G. Bischak acknowledges an NSF Graduate Research Fellowship (No. DGE1106400), and Naomi S. Ginsberg acknowledges a Packard Fellowship for Science and Engineering, a Camille Dreyfus Teacher-Scholar Award, and an Alfred P. Sloan Research Fellowship.

Electronic Supplementary Material: Supplementary material (detailed experimental methods, SEM images illustrating growth tunability, XRD, TEM characterization and CL spectrum of B-$CsPbI_3$ and Y-$CsPbI_3$ nanowires; optical and PL images of the B-$CsPbI_3$ and Y-$CsPbI_3$ nanowires for electrical measurement; XRD and PL characterization of the meta-stable phase of B-$CsPbI_3$ nanowires) is available in the online version of this article at http://dx.doi.org/10.1007/s12274-016-1415-0.

References

[1] Burschka, J.; Pellet, N.; Moon, S. J.; Humphry-Baker, R.; Gao, P.; Nazeeruddin, M. K.; Grätzel, M. Sequential deposition as a route to high-performance perovskite-sensitized solar cells. *Nature* **2013**, *499*, 316–319.

[2] Zhou, H. P.; Chen, Q.; Li, G.; Luo, S.; Song, T. B.; Duan, H. S.; Hong, Z. R.; You, J. B.; Liu, Y. S.; Yang, Y. Interface engineering of highly efficient perovskite solar cells. *Science* **2014**, *345*, 542–546.

[3] Dou, L. T.; Yang, Y. M.; You, J. B.; Hong, Z. R.; Chang, W.-H.; Li, G.; Yang, Y. Solution-processed hybrid perovskite photodetectors with high detectivity. *Nat. Commun.* **2014**, *5*, 5404.

[4] Jeon, N. J.; Noh, J. H.; Yang, W. S.; Kim, Y. C.; Ryu, S.; Seo, J.; Seok, S. I. Compositional engineering of perovskite materials for high-performance solar cells. *Nature* **2015**, *517*, 476–480.

[5] Niu, G. D.; Guo, X. D.; Wang, L. D. Review of recent progress in chemical stability of perovskite solar cells. *J. Mater. Chem. A* **2015**, *3*, 8970–8980.

[6] Leijtens, T.; Eperon, G. E.; Noel, N. K.; Habisreutinger, S. N.; Petrozza, A.; Snaith, H. J. Stability of metal halide perovskite solar cells. *Adv. Energy Mater.* **2015**, *5*, 1500963.

[7] Conings, B.; Drijkoningen, J.; Gauquelin, N.; Babayigit, A.; D'Haen, J.; D'Olieslaeger, L.; Ethirajan, A.; Verbeeck, J.; Manca, J.; Mosconi, E. et al. Intrinsic thermal instability of methylammonium lead trihalide perovskite. *Adv. Energy Mater.* **2015**, *5*, 1500477.

[8] Philippe, B.; Park, B. W.; Lindblad, R.; Oscarsson, J.; Ahmadi, S.; Johansson, E. M. J.; Rensmo, H. Chemical and electronic structure characterization of lead halide perovskites and stability behavior under different exposures? A photoelectron spectroscopy investigation. *Chem. Mater.* **2015**, *27*, 1720–1731.

[9] Protesescu, L.; Yakunin, S.; Bodnarchuk, M. I.; Krieg, F.; Caputo, R.; Hendon, C. H.; Yang, R. X.; Walsh, A.; Kovalenko, M. V. Nanocrystals of cesium lead halide perovskites ($CsPbX_3$, X = Cl, Br, and I): Novel optoelectronic materials showing bright emission with wide color gamut. *Nano Lett.* **2015**, *15*, 3692–3696.

[10] Zhang, D. D.; Eaton, S. W.; Yu, Y.; Dou, L. T.; Yang, P. D. Solution-phase synthesis of cesium lead halide perovskite nanowires. *J. Am. Chem. Soc.* **2015**, *137*, 9230–9233.

[11] Eaton, S. W.; Lai, M. L.; Gibson, N. A.; Wong, A. B.; Dou, L. T.; Ma, J.; Wang, L.-W.; Leone, S. R.; Yang, P. D. Lasing in robust cesium lead halide perovskite nanowires. *Proc. Natl. Acad. Sci. USA* **2016**, *113*, 1993–1998.

[12] Bekenstein, Y.; Koscher, B. A.; Eaton, S. W.; Yang, P. D.; Alivisatos, A. P. Highly luminescent colloidal nanoplates of perovskite cesium lead halide and their oriented assemblies. *J. Am. Chem. Soc.* **2015**, *137*, 16008–16011.

[13] Beal, R. E.; Slotcavage, D. J.; Leijtens, T.; Bowring, A. R.; Belisle, R. A.; Nguyen, W. H.; Burkhard, G. F.; Hoke, E. T.; McGehee, M. D. Cesium lead halide perovskites with improved stability for tandem solar cells. *J. Phys. Chem. Lett.* **2016**, *7*, 746–751.

[14] Møller, C. K. Crystal structure and photoconductivity of cæsium plumbohalides. *Nature* **1958**, *182*, 1436.

[15] Natarajan, M.; Prakash, B. Phase transitions in ABX_3 type halides. *Phys. Status Solidi A Appl. Res.* **1971**, *4*, K167–K172.

[16] Eperon, G. E.; Paterno, G. M.; Sutton, R. J.; Zampetti, A.; Haghighirad, A. A.; Cacialli, F.; Snaith, H. J. Inorganic caesium lead iodide perovskite solar cells. *J. Mater. Chem. A* **2015**, *3*, 19688–19695.

[17] Nedelcu, G.; Protesescu, L.; Yakunin, S.; Bodnarchuk, M. I.; Grotevent, M. J.; Kovalenko, M. V. Fast anion-exchange in highly luminescent nanocrystals of cesium lead halide perovskites (CsPbX_3, X = Cl, Br, I). *Nano Lett.* **2015**, *15*, 5635–5640.

[18] Swarnkar, A.; Marshall, A. R.; Sanehira, E. M.; Chernomordik, B. D.; Moore, D. T.; Christians, J. A.; Chakrabarti, T.; Luther, J. M. Quantum dot–induced phase stabilization of α-CsPbI_3 perovskite for high-efficiency photovoltaics. *Science* **2016**, *354*, 92–95.

[19] Dastidar, S.; Egger, D. A.; Tan, L. Z.; Cromer, S. B.; Dillon, A. D.; Liu, S.; Kronik, L.; Rappe, A. M.; Fafarman, A. T. High chloride doping levels stabilize the perovskite phase of cesium lead iodide. *Nano Lett.* **2016**, *16*, 3563–3570.

[20] Krumhansl, J. A.; Schrieffer, J. R. Dynamics and statistical mechanics of a one-dimensional model hamiltonian for structural phase transitions. *Phys. Rev. B* **1975**, *11*, 3535–3545.

[21] Gu, Q.; Falk, A.; Wu, J. Q.; Ouyang, L.; Park, H. Current-driven phase oscillation and domain-wall propagation in $W_xV_{1-x}O_2$ nanobeams. *Nano Lett.* **2007**, *7*, 363–366.

[22] Liu, W.; Pan, W.; Luo, J.; Godfrey, A.; Ou, G.; Wu, H.; Zhang, W. Suppressed phase transition and giant ionic conductivity in $La_2Mo_2O_9$ nanowires. *Nat. Commun.* **2015**, *6*, 8354.

[23] Campbell, M. G.; Powers, D. C.; Raynaud, J.; Graham, M. J.; Xie, P.; Lee, E.; Ritter, T. Synthesis and structure of solution-stable one-dimensional palladium wires. *Nat. Chem.* **2011**, *3*, 949–953.

[24] Trots, D. M.; Myagkota, S. V. High-temperature structural evolution of caesium and rubidium triiodoplumbates. *J. Phys. Chem. Solids* **2008**, *69*, 2520–2526.

[25] Stoumpos, C. C.; Kanatzidis, M. G. The Renaissance of halide perovskites and their evolution as emerging semiconductors. *Acc. Chem. Res.* **2015**, *48*, 2791–2802.

[26] Fu, Y. P.; Zhu, H. M.; Stoumpos, C. C.; Ding, Q.; Wang, J.; Kanatzidis, M. G.; Zhu, X. Y.; Jin, S. Broad wavelength tunable robust lasing from single-crystal nanowires of cesium lead halide perovskites (CsPbX_3, X = Cl, Br, I). *ACS Nano* **2016**, *10*, 7963−7972.

[27] Wang, Y. L.; Guan, X.; Li, D. H.; Cheng, H.-C.; Duan, X. D.; Lin, Z. Y.; Duan, X. F. Chemical vapor deposition growth of single-crystalline cesium lead halide microplatelets and heterostructures for optoelectronic applications. *Nano Res.*, in press, DOI: 10.1007/s12274-016-1317-1.

[28] Trigui, A.; Abid, H.; Mlayah, A.; Abid, Y. Optical properties and vibrational studies of a new self assembled organic–inorganic nanowire crystal $(C_6H_{13}N_3)_2Pb_3I_{10}$. *Synth. Met.* **2012**, *162*, 1731–1736.

[29] Wu, X. X.; Trinh, M. T.; Niesner, D.; Zhu, H. M.; Norman, Z.; Owen, J. S.; Yaffe, O.; Kudisch, B. J.; Zhu, X. Y. Trap states in lead iodide perovskites. *J. Am. Chem. Soc.* **2015**, *137*, 2089–2096.

[30] Bischak, C. G.; Sanehira, E. M.; Precht, J. T.; Luther, J. M.; Ginsberg, N. S. Heterogeneous charge carrier dynamics in organic−inorganic hybrid materials: Nanoscale lateral and depth-dependent variation of recombination rates in methylammonium lead halide perovskite thin films. *Nano Lett.* **2015**, *15*, 4799–4807.

[31] Li, D. H.; Wang, G. M.; Cheng, H. C.; Chen, C. Y.; Wu, H.; Liu, Y.; Duan, X. F. Size-dependent phase transition in methylammonium lead iodide perovskite microplate crystals. *Nat. Commun.* **2016**, *7*, 11330.

[32] Sutton, R. J.; Eperon, G. E.; Miranda, L.; Parrott, E. S.; Kamino, B. A.; Patel, J. B.; Hörantner, M. T.; Johnston, M. B.; Haghighirad, A. A.; Moore, D. T. et al. Bandgap-tunable cesium lead halide perovskites with high thermal stability for efficient solar cells. *Adv. Energy Mater.* **2016**, *6*, 1502458.

[33] Grote, C.; Berger, R. F. Strain tuning of tin−halide and lead−halide perovskites: A first-principles atomic and electronic structure study. *J. Phys. Chem. C* **2015**, *119*, 22832–22837.

[34] Zhang, H. Z.; Banfield, J. F. Thermodynamic analysis of phase stability of nanocrystalline titania. *J. Mater. Chem.* **1998**, *8*, 2073–2076.

[35] Hegedüs, J.; Elliott, S. R. Microscopic origin of the fast crystallization ability of Ge–Sb–Te phase-change memory materials. *Nat. Mater.* **2008**, *7*, 399–405.

[36] Ríos, C.; Stegmaier, M.; Hosseini, P.; Wang, D.; Scherer, T.; Wright, C. D.; Bhaskaran, H.; Pernice, W. H. P. Integrated all-photonic non-volatile multi-level memory. *Nat. Photonics* **2015**, *9*, 725–732.

[37] Li, P. N.; Yang, X. S.; Maß, T. W. W.; Hanss, J. L.; Lewin, M.; Michel, A.-K. U.; Wuttig, M.; Taubner, T. Reversible optical switching of highly confined phonon–polaritons with an ultrathin phase-change material. *Nat. Mater.* **2016**, *15*, 870–875.